Journal of Solid State Chemistry 183 (2010) 1678–1690

Contents lists available at ScienceDirect

Journal of Solid State Chemistry

journal homepage: www.elsevier.com/locate/jssc

# Effect of electron correlation in $Sr(Ca)Ru_{1-x}Cr_xO_3$: Density functional calculation

H. Hadipour, M. Akhavan *

*Magnet Research Laboratory (MRL), Department of Physics, Sharif University of Technology, P.O. Box 11365-9161, Tehran, Iran*

ARTICLE INFO

*Article history:*
Received 8 March 2010
Received in revised form
11 May 2010
Accepted 11 May 2010
Available online 15 May 2010

*Keywords:*
Ruthenates
Strongly correlated systems
Ferromagnetic materials

ABSTRACT

We have investigated the electronic structure of $Sr(Ca)Ru_{1-x}Cr_xO_3$ using the full potential linearized augmented plane wave method by different approximation such as LSDA and LSDA+$U$. The LSDA calculation suggest that $Cr^{4+}$–$Ru^{4+}$ hybridization is responsible for the high Curie temperature $T_C$ in $SrRu_{1-x}Cr_xO_3$, but it cannot completely describe its physical behavior. Our LSDA+$U$ DOS results for $SrRu_{1-x}Cr_xO_3$ clearly establishes renormalization of the intra-atomic exchange strength at the Ru sites, arising from the Cr–Ru hybridization. The antiferromagnetic coupling of $Cr^{3+}$ with $Ru^{4+,5+}$ lattice increases the screening, which is consistent with the low magnetic moment of the Ru ions. The more distorted Ca-based compounds as compared to the Sr-based systems shows that the hybridization mechanism is not relevant for these compounds. The bigger exchange splitting of Ru 4$d$ and Cr 3$d$ at the Fermi level with $Ru^{4+,5+}$ and $Cr^{3+,4+}$ orbital occupancies of $CaRu_{0.75}Cr_{0.25}O_3$ in the LSDA+$U$ calculation, compared with that of the LSDA calculation, shows that repulsion between electrons tend to keep the localized spins from overlapping. The low screening of the Ru $t_{2g}$ electrons increases $T_C$ in the Ca-based systems, which is consistent with the both high Ru exchange splitting and magnetic moment. The insulating behavior of the high Cr-doped systems can be explained by considering the $Ru^{4+}+Cr^{4+}\rightarrow Ru^{5+}+Cr^{3+}$ charge transfer.



## 1. Introduction

The transition metal compounds with 4$d$ orbitals may show both features of the localized and itinerant electrons. With some results from computational methods such as the local spin density approximation (LSDA), due to the large spatial extent of the 4$d$ orbitals with the total bandwidth of about 3–4 eV, the electron–electron correlation effect becomes less important compared to the strong hybridization. But, the LSDA+$U$ calculations indicate the importance of the electron correlation effects in the valence band. These two approaches may be considered as two limiting cases: LSDA is more suitable for materials with itinerant electrons, and in contrast, LSDA+$U$ is widely used for description of the systems with localized electrons.

$SrRuO_3$ is metallic and shows ferromagnetism (FM) below $T_C$=165 K with a saturation moment between 0.8 and 1.6 $\mu_B$/Ru [1–3]. According to density functional calculations with LSDA, $SrRuO_3$ is an itinerant ferromagnetic (FM) metal with its magnetism arising from the Stoner instability [4–6]. On the other hand, $CaRuO_3$ forms in the same crystal structure and symmetry as $SrRuO_3$, but due to the ionic size mismatch between the Ca and Ru ions, it yields a state less favorable for FM, so $CaRuO_3$ is a metallic paramagnet (PM) [3,2]. The octahedral crystalline electric field (CEF) of the O atoms splits the fivefold degeneracy of the Ru $4d^4$ configuration into a two-thirds occupied triplet ($t_{2g}$) ground state, and an unoccupied doublet ($e_g$) excited state. The highly extended 4$d$ electrons and the $t^3_{2g\uparrow}t^1_{2g\downarrow}$ electronic configuration is responsible for the magnetic and transport properties of these materials [4].

On the other hand, some spectroscopic results indicate that $Sr(Ca)RuO_3$ should be considered as a strongly correlated electron system [8,7,9,10]. The optical spectroscopic studies have revealed that $Sr(Ca)RuO_3$ is a non-Fermi liquid system [12,13,11], and $CaRuO_3$ is a PM metal with the low-temperature conductivity very close to the Mott minimum value [7]. Furthermore, some studies have predicted an antiferromagnetic (AFM) ordering in $CaRuO_3$ [14]. So, these evidences suggest that $CaRuO_3$ is near to the metal–insulator (Mott insulator) transition boundary. Also, due to $SrRuO_3$ and $CaRuO_3$ having similar electronic properties and states, Rondinelli and coworkers [15] have calculated the DOS with LSDA+$U$ with $U$= 1.0 eV both for bulk and thin film of $SrRuO_3$. They have confirmed that inclusion of correlations causes a significant role in determining the magnetic properties of the system compared with the LSDA results. For other ruthenate system, $Sr_2RuO_4$ is metallic and tends to be FM with $p$-wave superconductivity [1]. In addition, the high-resolution angle-resolved photoemission spectroscopy suggest that some ruthenium oxides should be

* Corresponding author. Fax: +98 21 66012983.
*E-mail address:* akhavan@sharif.edu (M. Akhavan).

0022-4596/$ - see front matter © 2010 Elsevier Inc. All rights reserved.
doi:10.1016/j.jssc.2010.05.013

considered as strongly correlated electron systems [8]. For example, $Ca_3Ru_2O_7$ and $Ca_2RuO_4$ can be thought of as a typical AFM Mott-insulator, while $Sr_3Ru_2O_7$ is shown to be metallic.

Substitution of the Ru ions by the impurity ions extensively destroys the magnetic ground state in $CaRu_{1-x}Sn_xO_3$ [16], $CaRu_{1-x}Rh_xO_3$ [17], $SrRu_{1-x}Mn_xO_3$ [18], other impurity doped $CaRuO_3$ [19] and $SrRuO_3$ compounds [20,22,23,21,24]. Also, the Mn doping in $SrRu_{1-x}Mn_xO_3$ drives the system from the itinerant FM state with $T_C=165$ K for $x=0$ through a critical point at $x_c=0.39$ to an insulating AFM state [18]. The exception found to increase $T_C$ is substitution of Cr or Pb on the Ru site [16]. $SrRu_{1-x}Cr_xO_3$ shows an increase in $T_C$ to 188 K for $x=0.11$. Cr substitution as low as $x=0.08$ drives $CaRu_{1-x}Cr_xO_3$ from PM to FM state. The FM occurs abruptly and $T_C$ reaches as high as 123 K for $x=0.22$. For both $SrRu_{1-x}Cr_xO_3$ and $CaRu_{1-x}Cr_xO_3$, on the basis of the magnetic susceptibility and electrical resistivity measurements [20,25–27], the transition to the new or stronger magnetic state is found to be accompanied by a metal to insulator transition. The double exchange (DE) interaction due to the creation of $Ru^{4+/5+}$–$O_2$–$Cr^{4+/3+}$ configuration, possibilitates $Cr^{3+}$ and $Cr^{4+}$ to attain magnetic ordering, by which it enhances the ordering temperature [25]. The supercell calculations for Cr substitutions for Ru in $SrRuO_3$ indicate that due to the strong hybridization between the majority spin Cr $t_{2g}$ orbitals and O $p$–Ru $t_{2g}$ bands, AFM alignment of the Cr moments with the host lattice magnetization takes place [28].

The large CEF splitting due to the extension of the Ru 4$d$ orbitals yields a low spin state with $S=1$ in Sr(Ca)$RuO_3$. On the other hand, the Cr ions have the trivalent $3d^3$ $Cr^{3+}$ or the tetravalent $3d^2$ $Cr^{4+}$ state electron configuration. Two of the three $t_{2g}$ orbitals are occupied for $Cr^{4+}$, but each of the three $t_{2g}$ orbitals is half filled for $Cr^{3+}$. The $CaCrO_3$ and $SrCrO_3$ perovskite respective structures create an insulating AFM and a metallic PM state [29,30]. Also, from the LSDA and LSDA+$U$ calculations, Streltsov and coworkers [31] have concluded that $CaCrO_3$ is in a crossover regime between the localized and itinerant electrons. In the $CaRuO_3$, due to relatively small size of $Ca^{2+}$, the $RuO_6$ octahedra are tilted which in turn lead to weak hybridization between the Ru and O electrons resulting in AF ordering [14]. Therefore, one may consider $CaRuO_3$ as a compound with intermediate correlation strength like $CaCrO_3$, lying at the edge of the metal–insulator transition boundary.

The variation of the magnetic structure leads to a complex pattern of the changes in the electronic structure. This pattern depends on the energy position of the states, spin polarization, and hybridization. Although DFT is one of the best approaches to describe the ground state properties of systems, the description of finite temperature, such as $T_C$, is not straightforward. In the framework of mean-field approximation (MFA), $T_C$ for the multiple sub-lattices is calculated as the largest eigenvalue of the equation $\det(T_{pq}-T\delta_{pq})=0$, where $p$ and $q$ are the indices of the nonequivalent magnetic sub-lattices, and $T_{pq}=2J^0_{pq}/3K_B$ [32]. $J^0_{pq}$ is an effective interaction of an atom from sublattice $p$ with all other atoms from the sublattice $q$. The random-phase approximation (RPA) is supposed to give better estimation of $T_C$. The RPA approach to the calculation of $T_C$ of multiple-sublattice systems is discussed in Ref. [33]. They arrived at the following formula:

$$k_BT_C=\frac{2}{3\langle s^z_m\rangle}\frac{S_m+1}{S_m}\frac{1}{\Omega}\int dq[N^{-1}(q)_{mm}]^{-1}, \quad (1)$$

where $k_B$ is the Boltzmann constant, $s^z_m$ is the $z$ component of the spin of the site $m$, and $S_m$ is the value of the spin of the atoms of the $m$ type. $[N^{-1}(q)_{mm}]$ in Eq. (1) is the diagonal element of the matrix inverse to matrix $N$ defined by

$$N_{mn}=\delta_{mn}\left[\Delta+\sum_k J_{mk}(0)\langle s^z_k\rangle\right]-J_{mn}(q)\langle s^z_m\rangle, \quad (2)$$

where $\Delta$ gives the magnetic anisotropy energy. $N_{mn}$ is a function of $V$ (hybridization between local and itinerant states). Sharma et al. [34] solved Eq. (1) within a self-consistent cycle and indicated that the value of $T_C$ is higher and increases with increasing the hybridization strength. Also, Sarma et al. [35] have shown that the Fe–Mo hybridization induces exchange splitting which is responsible for the high $T_C$ in $Sr_2FeMoO_6$. Also, Sandratskii et al. [36] have estimated $T_C$ in the MFA discussed above for the GaMnN and GaMnAs systems; the carrier number and the efficiency of the screening of the on-site Coulomb interaction are important characteristics in the $T_C$ of these systems.

On the other hand, the difference in the magnetic and non-magnetic phases can be explained on the basis of the Stoner criterion [38], which states that a non-magnetic state of a system is unstable with respect to the formation of the ferromagnetic state if $I(N(E_F))>1$, and it is stable if this value is smaller than one. Also, the exchange splitting is a general function of magnetization $m(r)$, $E_{ES}=V_\uparrow-V_\downarrow=\partial E^{LSDA}/\partial n_\uparrow(r)-\partial E^{LSDA}/\partial n_\downarrow(r)=m(r)f(r)$. For small magnetization, the exchange splitting is independent of $k$, and we can write $\langle\Psi_k|m(r)f(r)|\Psi_k\rangle=mI$ [39]. So, the Stoner parameter can be estimated according to the formula: $I=E_{ES}/m$, where $E_{ES}$ is the exchange splitting between spin-up and spin-down states and $m$ is the corresponding magnetic moment giving the origin to the exchange splitting. The value of $E_{ES}$ is estimated from the DOS as the energy distance between corresponding peaks in the spin-up and spin-down DOSs. Sarma et al. indicated that the bare $I$ at the Mo site must be strongly renormalized giving rise to an enhanced $I_{eff}$ leading to the pronounced spin polarization of the Mo $d$ bands [35]. So, although we cannot directly predict the values of the exchange parameters by the analysis of the electronic DOS of the ground state, to get an insight into the role of the Cr atoms in the Sr(Ca)$Ru_{1-x}Cr_xO_3$, it is instructive to compare the variation in the electron structure for a series of these systems.

In attempt to understand the large increase of $T_C$ in the Cr-doped Sr(Ca)$Ru_{1-x}Cr_xO_3$ and the effect of electron correlation, we report the results of the electronic structure calculation for the Sr(Ca)$Ru_{1-x}Cr_xO_3$ compounds. We have chosen the Ca(Sr)$Ru_{0.75}Cr_{0.25}O_3$ systems due to the optimum doping (maximum $T_C$ for $x\approx0.25$) [26,27]. Applying correlation confirms that large increase of $T_C$ in $SrRu_{1-x}Cr_xO_3$ is due to the antiparallel orientation between the Cr and Ru states. Also, inclusion of correlations causes a significant role in revealing the magnetic properties of $CaRu_{1-x}Cr_xO_3$; due to the more distorted structure, the mechanism is different in the Ca-based system, where the low screening strengthens the exchange coupling between the local spins, and increases $T_C$.

## 2. Theoretical methods

We have calculated the spin polarized electronic structure of Sr(Ca)$Ru_{1-x}Cr_xO_3$ using the full-potential linearized augmented plane-wave (FLAPW) [40] method within the LSDA and LSDA+$U$ approximation with WIEN2K software [41]. Additional local orbitals (LO) were used for all semicore states [42]. In the LSDA calculation, we have used the Perdew–Wang parameters for the exchange and correlation functional. The experimental results show that the orthorhombic symmetry is retained as a function of $x$ in the low doping regime [26,27]. In all calculations the lattice parameters (structure shown in Fig. 1) were chosen to be equal to the relaxed computational lattice parameter of Sr(Ca)$Ru_{1-x}Cr_xO_3$ with orthorhombic *Pbma* space group. The unrelaxed lattice parameters were chosen from the experimental lattice parameters of Sr(Ca)$RuO_3$ and Sr(Ca)$Ru_{1-x}Cr_xO_3$ [43,26,27]. The muffin-tin radii (RMT) for Sr/Ca, Ru/Cr, and O were set to 0.95, 0.80, and 0.75 Å, respectively. The convergence for different calculations was achieved considering 500 k points within the

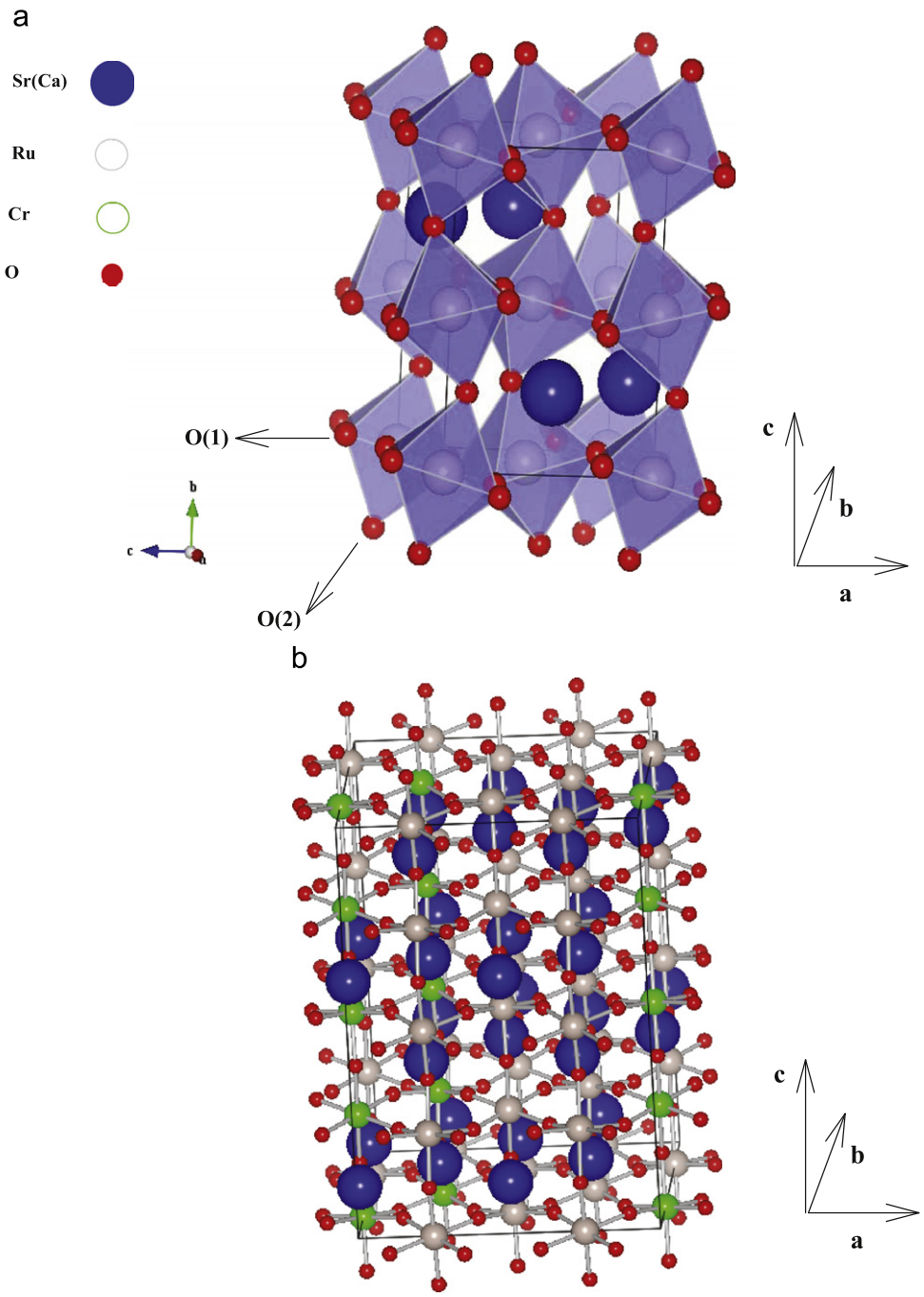


**Fig. 1.** The *Pbnm* crystal structure of $Sr(Ca)RuO_3$ (a), and $Sr(Ca)Cr_{0.25}Ru_{0.75}O_3$ supercell (b). The thick solid lines show the Ru(Cr)–O–Ru(Cr) bands.

first Brillouin zone. The error bar for the energy convergence was set to 0.1 meV per formula unit. In every case, the charge convergence was achieved to be less than 0.001 electronic charge.

The calculations for $Sr(Ca)Ru_{0.75}Cr_{0.25}O_3$ are based on the supercell approach with the Cr moment antiparallel (AP) to the Ru magnetization. The supercell is a doubled cell $2\times2\times2$ of the experimental structure of $CaRuO_3$ and $SrRuO_3$ which for example for every four Ru atoms one Ru is replaced by Cr, corresponding to 25 percent Cr substitution. There are Cr–O–Cr bonds, but there is no $CrO_6$ octahedra in the supercell. The Ru ions in the supercell have two configurations: Ru(1) with six Ru neighbors and Ru(2) with four Cr and two Ru neighbors. The $2\times2\times2$ crystallographic structure of the orthorhombic *Pbnm* $Sr(Ca)Ru_{1-x}Cr_xO_3$ ($x$=0.25) compound is given in Fig. 1(b).

In the LSDA+$U$ method [44], we have used the Coulomb interaction between the localized Cr 3$d$ and Ru 4$d$ electrons in the spirit of a mean-field Hubbard model, whereas the interactions between the less localized $s$ and $p$ electrons are treated within the LSDA approximation. We have used the rotationally invariant scheme of LSDA+$U$ functional which can be written as the following:

$$E_{LSDA+U}=E_{LSDA}+E_U-E_{dc} \tag{3}$$

where

$$E_U=\tfrac{1}{2}\sum_{m,\sigma}\langle m,m''|V_{ee}|m',m'''\rangle\rho^{\sigma}_{m,m'}\rho^{-\sigma}_{m'',m'''}+(\langle m,m''|V_{ee}|m',m'''\rangle -\langle m,m''|V_{ee}|m''',m'\rangle)\rho^{\sigma}_{m,m'}\rho^{\sigma}_{m'',m'''} \tag{4}$$

and

$$E_{dc} = \frac{1}{2}Un(n-1) - \frac{1}{2}J\sum_{\sigma} n^{\sigma}(n^{\sigma}-1), \quad (5)$$

with $n = n^{\uparrow} + n^{\downarrow}$, $n_{\sigma} = Tr\rho^{\sigma}$, and $V_{ee}$ is the screened Coulomb interaction among the $d$ electrons. The LSDA+$U$ approach adds the orbital-dependent Coulomb interaction $E_U$ to LSDA and additional double counting correction $E_{dc}$ is introduced to subtract that part of the electron–electron interaction between the localized orbitals that is already included in the LSDA [44]. We have used the fully localized limit (self-interaction corrected) approximation to introduce the double counting term in this work.

The parameters of the electron–electron interaction for Ca(Sr)$Ru_{1-x}Cr_xO_3$ perovskites have been estimated for localization of the Ru 4$d$ and Cr 3$d$ electrons by using the standard LSDA-constraint technique [45–47]. The meaning of the $U$ parameter is defined as the cost in Coulomb energy by placing two electrons on the same site. The $U$ corresponds to $F^0$ of the unscreened Slater integrals in an atom [48]. Due to screening, the effective $U$ ($U_{eff}$) in solids is much smaller than $F^0$ for atoms. To calculate the $U_{eff}$ and $J_{eff}$, similar to Anisimov and Gunnarsson's work [48], we consider a large finite 8-unit supercell in which the $d$ charge on one atom is constrained and the eigenvalue is obtained. The values of $U_{eff}$ and $J_{eff}$ depend on how one constraints the $d$ shells. All of the 3$d$ and 4$d$ electrons on one of the atoms in the supercell is localized, so, we fixed the occupancies of the $d$ shell of the central atom at two values ($n/2+1/2$, $n/2$) and ($n/2+1/2$, $n/2-1$), and $U_{eff}$ and $J_{eff}$ are then deduced from

$$F^0_{eff} = U_{eff} = \varepsilon_{3d\uparrow}((n/2+1/2),n/2) - \varepsilon_{3d\uparrow}((n/2+1/2),n/2-1) - \varepsilon_F((n/2+1/2),n/2) + \varepsilon_F((n/2+1/2),n/2-1) \quad (6)$$

$$J = J_{eff} = \varepsilon_{3d\uparrow}((n/2+1/2),n/2) - \varepsilon_{3d\downarrow}((n/2+1/2),n/2-1) - \varepsilon_F((n/2+1/2),n/2) + \varepsilon_F((n/2+1/2),n/2-1). \quad (7)$$

How should $F^0_{eff}$ be used to calculate $U$ in the LSDA+$U$ calculation? The orbital-dependent potentials entering the Kohn–Sham equation that arise from the $H_U$ and $H_{dc}$ shows that an occupied and an unoccupied orbital will be split by $U_{eff}=U-J$ [49]. As the screening of $F^2$ and $F^4$ in solids appears to be small, $J_{eff}=J$ can be calculated from the atomic values. So, to explore the correlation effects in the 3$d$ orbitals, we used the Coulomb energy $U=U_{eff}+J=4.0$ eV (3.0 eV) and exchange parameter $J=J_{eff}=1.5$ eV (1.5 eV) for Cr ions in the Ca-based (Sr-based) systems, whereas we used $U=2.9$ eV for the Ru ions due to the nearly itinerant valence 4$d$ orbitals.

## 3. Results and discussion

The volume of the unit cell as well as the atomic coordinates for each configuration are optimized. Table 1 shows both the experimental and computational lattice parameters ($a$, $b$, and $c$), and atomic positions for *Pbnm* space group configuration of Sr(Ca)$Ru_{0.75}Cr_{0.25}O_3$. For $x=0$ (both $SrRuO_3$ and $CaRuO_3$), the orthorhombic *Pbnm* configuration is stable with 0.52 eV/unit cell and 0.4 eV/unit cell energy lower than tetragonal $I$ 4/$mcm$ configuration and the optimized lattice parameters (not shown) are in good agreement with the experimental values [50,43]. For $x=0.25$ Sr-based (Ca-based), the optimized lattice parameters with $|\Delta a|/a = 0.47\%$ ($|\Delta a|/a = 0.64\%$), $|\Delta b|/b = 0.55\%$ ($|\Delta b|/b = 0.16\%$), and $|\Delta c|/c = 0.02\%$ ($|\Delta c|/c = 1.2\%$) are in good agreement with the experiment [50]. For the charge balance state Sr(Ca)$(Ru^{4+}_{1-x}Cr^{4+}_x)O_3$ ($Cr^{4+}$ and $Ru^{4+}$ with respective ionic radii of 0.55 Å and 0.62 Å), the calculated lattice parameters should decrease sharply with $x$. In our calculation, the reduction of volume ($|\Delta V|/V$) are 1.15% and 1.70% for the Sr- and Ca-based, respectively. The experimental values of the lattice parameters specially for the Ca-based system shown in Table 1 demonstrate a slight decrease with increasing $x$ ($|\Delta V|/V = 0.91\%$) similar to our calculation for both Sr- and Ca-based systems. So, Sr- and Ca-based systems are closer to the charge balance of $Sr(Ru^{4+,5+}_{1-x}Cr^{4+,3+}_x)O_3$ and creation of $Cr^{3+}$ (ionic radii of 0.615 Å) in the systems.

The Ru–O–Ru angle has significant influence in the effective electron correlation $U/W$ ($W=d$ bandwidth). As shown in Fig. 1(a), O(1) represents the apical oxygen in the $RuO_6$ octahedra along the $z$ axis in the structure and O(2) represents the oxygens in the basal $xy$ plane. In $SrRuO_3$, the Ru–O(1)–Ru and Ru–O(2)–Ru angles are respectively 167.6° and 159.7° [51], and also 162.85° and 162.81° from Ref. [26]. $CaRuO_3$ is a more distorted structure [52], and its respective angles are Ru−O(1)−Ru = 149.6° and Ru−O(2)−Ru = 149.8° [53]. The experimental results however show that increasing Cr reduces the structural distortion in the Sr-based system (increasing the Ru–O(1)–Ru and Ru–O(2)–Ru bond angles to 166.90° and 165.20°, respectively) of the perovskite cell due to its smaller ionic radii as compared to Ru.

**Table 1**
Unit-cell dimensions ($a$, $b$, and $c$), atomic position ($x$, $y$, and $z$), and bond angles of orthorhombic *Pbnm* space group of Sr(Ca)$Ru_{0.75}Cr_{0.25}O_3$: experimental results (ER) and present computational work (PCW).

| Formula | $SrRuO_3$ ER [26] | $CaRuO_3$ ER [27,53] | Sr(Ca)$Ru_{0.75}Cr_{0.25}O_3$ ER [26,27] | $SrRu_{0.75}Cr_{0.25}O_3$ PCW | $CaRu_{0.75}Cr_{0.25}O_3$ PCW |
|---|---|---|---|---|---|
| $a$ (Å) | 5.571 | 5.420 | 5.547(5.410) | 5.521 | 5.445 |
| $b$ (Å) | 5.533 | 5.534 | 5.514(5.501) | 5.545 | 5.492 |
| $c$ (Å) | 7.848 | 7.670 | 7.809(7.660) | 7.811 | 7.562 |
| Sr(Ca) $x$ | 0.950 | 0.922 | 0.946 | 0.984 | 0.942 |
| $y$ | 0.250 | 0.250 | 0.250 | 0.250 | 0.250 |
| $z$ | 0.010 | 0.012 | 0.010 | 0.003 | 0.014 |
| Ru(Cr) $x$ | 0.000 | 0.000 | 0.000 | 0.000 | 0.000 |
| $y$ | 0.000 | 0.000 | 0.000 | 0.000 | 0.000 |
| $z$ | 0.500 | 0.500 | 0.500 | 0.500 | 0.500 |
| O(1) $x$ | 0.022 | 0.020 | 0.024 | 0.003 | 0.029 |
| $y$ | 0.250 | 0.250 | 0.250 | 0.250 | 0.250 |
| $z$ | 0.549 | 0.589 | 0.534 | 0.526 | 0.603 |
| O(2) $x$ | 0.216 | 0.203 | 0.227 | 0.223 | 0.202 |
| $y$ | 0.511 | 0.451 | 0.491 | 0.507 | 0.447 |
| $z$ | 0.201 | 0.203 | 0.208 | 0.209 | 0.198 |
| Ru–O(1)–Ru (deg) | 162.85 | 149.6 | 166.90 | 165.79 | 146.40 |
| Ru–O(2)–Ru (deg) | 162.81 | 149.8 | 165.20 | 164.72 | 147.98 |

For the Sr-based system, our calculation is consistent with the experimental results [26] and increase of $T_C$ with Cr substitution, which may be related to a smaller deviation of the Ru(Cr)–O–Ru(Cr) bond angle. In $CaRu_{0.75}Cr_{0.25}O_3$, the Ru–O(1)–Ru and Ru–O(2)–Ru bond angles is very close to the $CaRuO_3$ case, and also decreases with more Cr substitution, which suggests that electron correlation may be an important element in the Ca-based compounds. So, we first compare the two $SrRu_{1-x}Cr_xO_3$ and $CaRu_{1-x}Cr_xO_3$ phases by the LSDA method, and later we will point out the results by the LSDA+$U$ method.

### 3.1. LSDA calculation of $SrRuO_3$ and $SrRu_{0.75}Cr_{0.25}O_3$

To compare the contributions of Cr to the ruthenate electronic structures, we have performed the electronic structure calculations for *Pbnm*-type $SrRuO_3$ and $SrRu_{0.75}Cr_{0.25}O_3$ in the LSDA using the FLAPW. The AP alignment phase has the lowest total energy as compared to the FM and non-magnetic phase, which is in agreement with the both computational and experimental findings [26–28], noting that in all cases the Cr moment aligns antiparallel to the Ru magnetization. Symmetry directions of the Brillouin zone (BZ) and the band structures along the high-symmetry directions of the BZ are shown in Figs. 2(a) and (b), respectively. The partial DOS for $SrRuO_3$ and $SrRu_{0.75}Cr_{0.25}O_3$ are shown in Figs. 3(a) and (b).

The Sr electronic states contribute in the energy range of 5 to 8.5 eV above the Fermi level with almost no contribution at lower energies (not shown). The O 2$p$ PDOS (inset to Figs. 3(a) and (b)) also has finite contributions in this energy range suggesting finite mixing between the O 2$p$ and Ru 4$d$ electronic states. A remarkable feature of DOS in $SrRuO_3$ is that the O 2$p$ states are heavily involved. So, the magnetism arises from a Stoner instability, which in turn results from a high DOS derived from the Ru $4dt_{2g}$–O 2$p$ hybridized bands around the Fermi energy $E_F$. This is consistent with the results that only 2/3 of the magnetization is from Ru 4$d$ [6,5], which is due to the strong

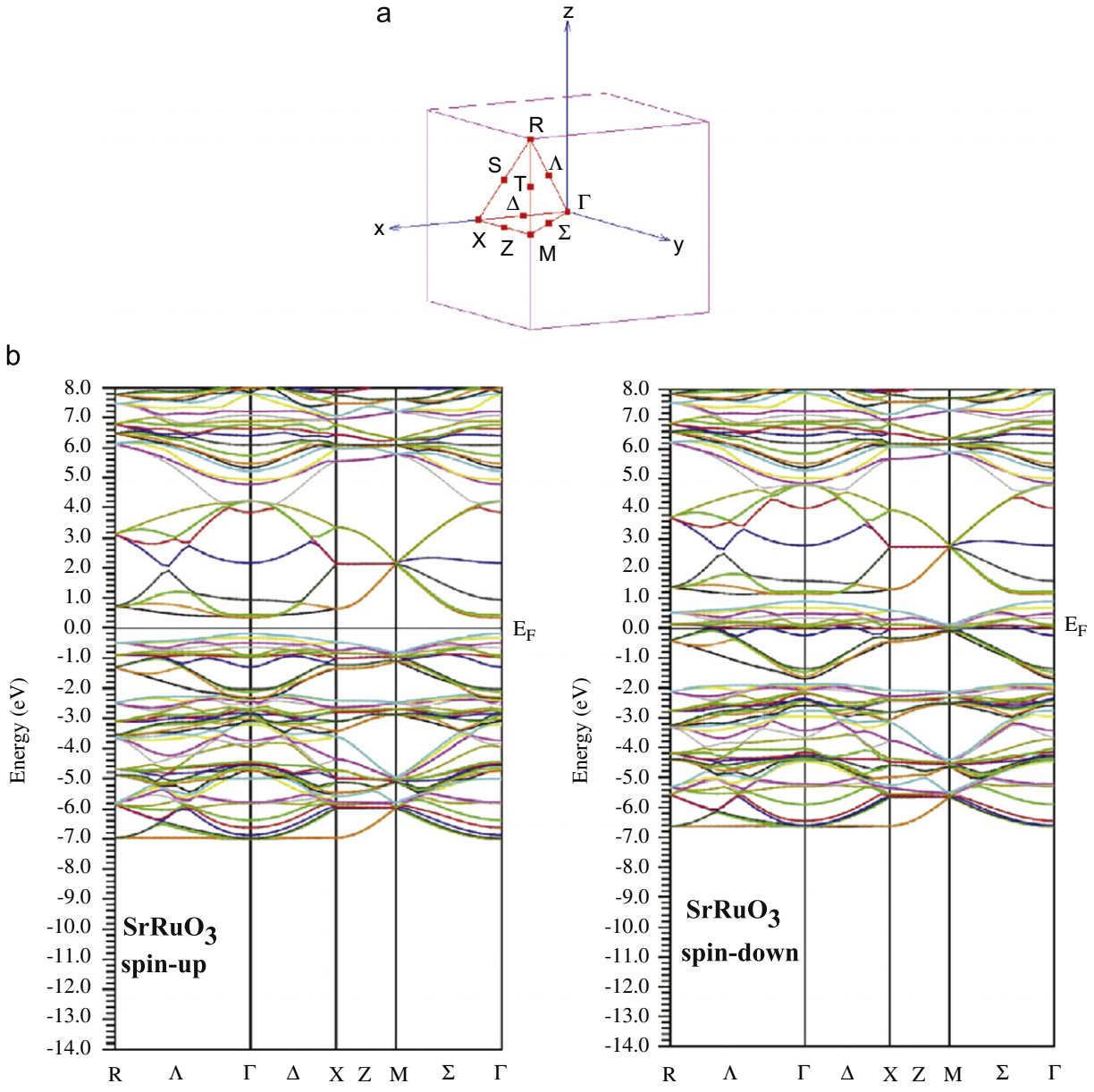


**Fig. 2.** (a) Symmetry directions of the BZ. (b) The band structure computed with the LSDA method along some high-symmetry directions for FM $SrRuO_3$. The position of the Fermi energy is indicated at zero.

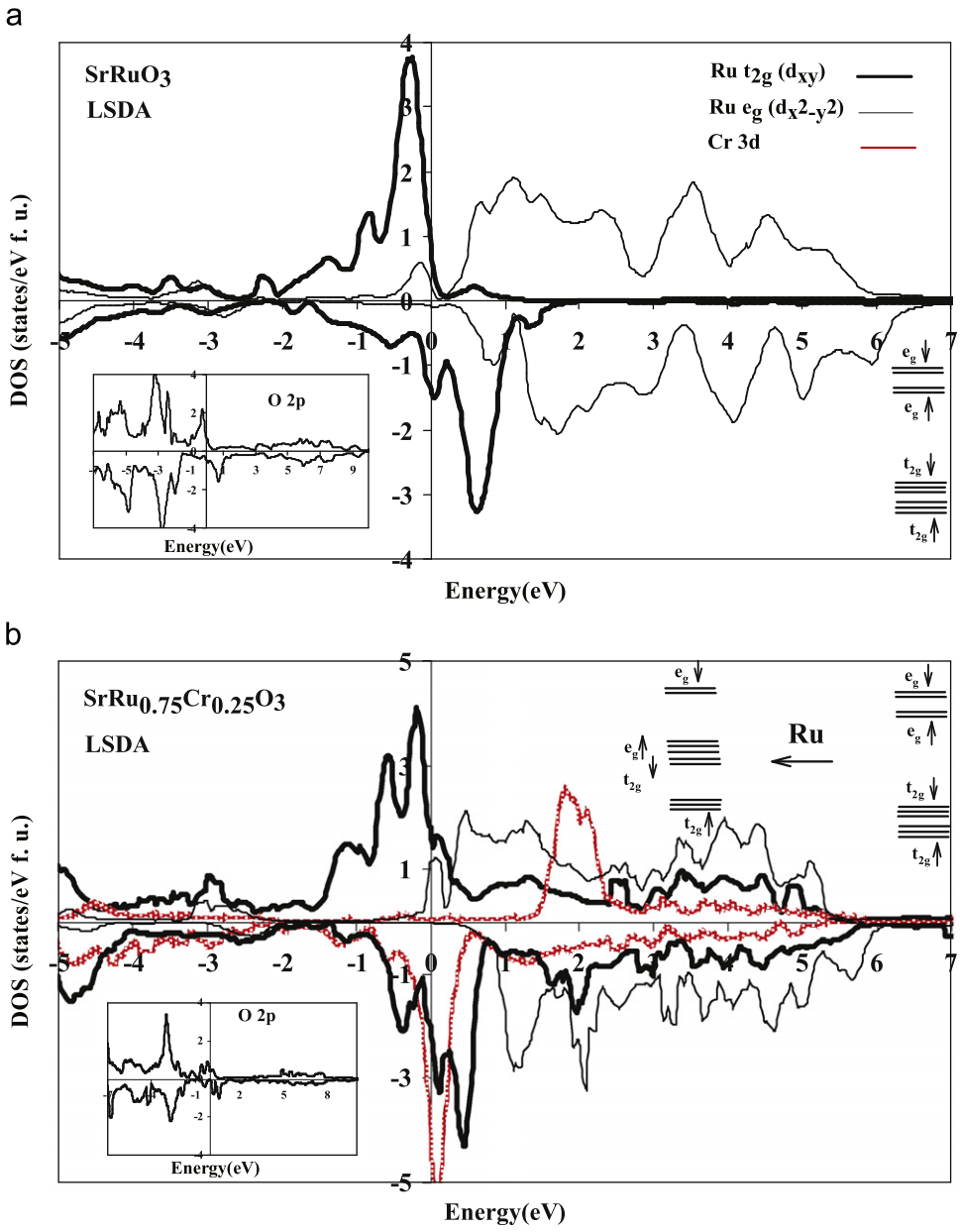


**Fig. 3.** The PDOS calculated by LSDA for (a) $SrRuO_3$ and (b) $SrCr_{0.25}Ru_{0.75}O_3$. In both calculations the position of the Fermi energy is indicated at zero. The DOS results are presented for two spins: up (down) panel corresponding to the spin majority (minority). The O 2*p* PDOS are shown in the inset to Figs. 3(a) and (b).

**Table 2**
Electronic parameters for $Sr(Ca)Ru_{1-x}Cr_xO_3$ perovskites deduced from DOS: crystal electric field (CEF), exchange splitting (ES), bandwidth (*W*).

| Formula (approximation) | Ru(CEF) (eV) | Cr(CEF) (eV) | Ru(ES) (eV) | Cr(ES) (eV) | Ru $t_{2g}$(W) (eV) | Cr $t_{2g}$(W) (eV) |
|---|---|---|---|---|---|---|
| $SrRuO_3$ (LSDA) | 1.50 | – | 1.10 | – | 3.50 | – |
| $CaRuO_3$ (LDA) | 2.00 | – | – | – | 3.10 | – |
| $SrRu_{0.75}Cr_{0.25}O_3$ (LSDA) | 0.30 | 0.40 | 0.80 | 2.00 | 3.20 | 2.20 |
| $SrRu_{0.75}Cr_{0.25}O_3$ (LSDA+*U*) | 0.30 | 0.40 | 1.50 | 2.20 | 3.30 | 2.00 |
| $CaRu_{0.75}Cr_{0.25}O_3$ (LSDA) | 1.20 | 0.50 | 0.90 | 2.20 | 3.00 | 2.00 |
| $CaRu_{0.75}Cr_{0.25}O_3$ (LSDA+*U*) | 1.30 | 0.50 | 2.1 | 2.00 | 3.00 | 2.20 |

hybridization between Ru and O. The PDOS corresponding to Ru orbitals spreads over a large energy range of −2 to 6.5 eV, which in turn confirms the strong hybridization between the Ru 4*d* and O 2*p* orbitals in $SrRuO_3$. This is also consistent with the other band structure calculations which indicate that the 4*d* orbital is quite extended and makes strong bonding [5,6]. So, from the LSDA calculation and due to the large spatial extent of the 4*d* orbitals in the $SrRuO_3$, the electron–electron correlation effect becomes less important than the strong hybridization with *W* of about 3.5 eV. This effect causes more screening and a reduced Hubbard *U*.

The *d* orbitals split into doubly degenerate $e_g$-like ($d_{z^2}$ and $d_{x^2-y^2}$) and triply degenerate localized $t_{2g}$-like ($d_{xy}$, $d_{xz}$, and $d_{yz}$) states. As shown in Fig. 3(a), the DOS intensity at Fermi energy

**Table 3**
Electronic parameters for $Sr(Ca)Ru_{1-x}Cr_xO_3$ perovskites deduced from DOS: magnetic moment (MM), orbital occupancy (OO).

| Formula (approximation) | Ru(MM) ($\mu_B$/Ru) | Cr(MM) ($\mu_B$/Cr) | Ru(OO) (e) | Cr(OO) (e) |
|---|---|---|---|---|
| $SrRuO_3$ (LSDA) | 1.16 | – | 4.0 | – |
| $CaRuO_3$ (LDA) | – | – | 4.0 | – |
| $SrRu_{0.75}Cr_{0.25}O_3$ (LSDA) | 1.05 | −1.92 | 3.80 | 2.10 |
| $SrRu_{0.75}Cr_{0.25}O_3$ (LSDA+$U$) | 1.08 | −2.08 | 3.10 | 2.90 |
| $CaRu_{0.75}Cr_{0.25}O_3$ (LSDA) | 1.24 | −1.93 | 3.80 | 2.10 |
| $CaRu_{0.75}Cr_{0.25}O_3$ (LSDA+$U$) | 1.36 | −2.23 | 3.60 | 2.50 |

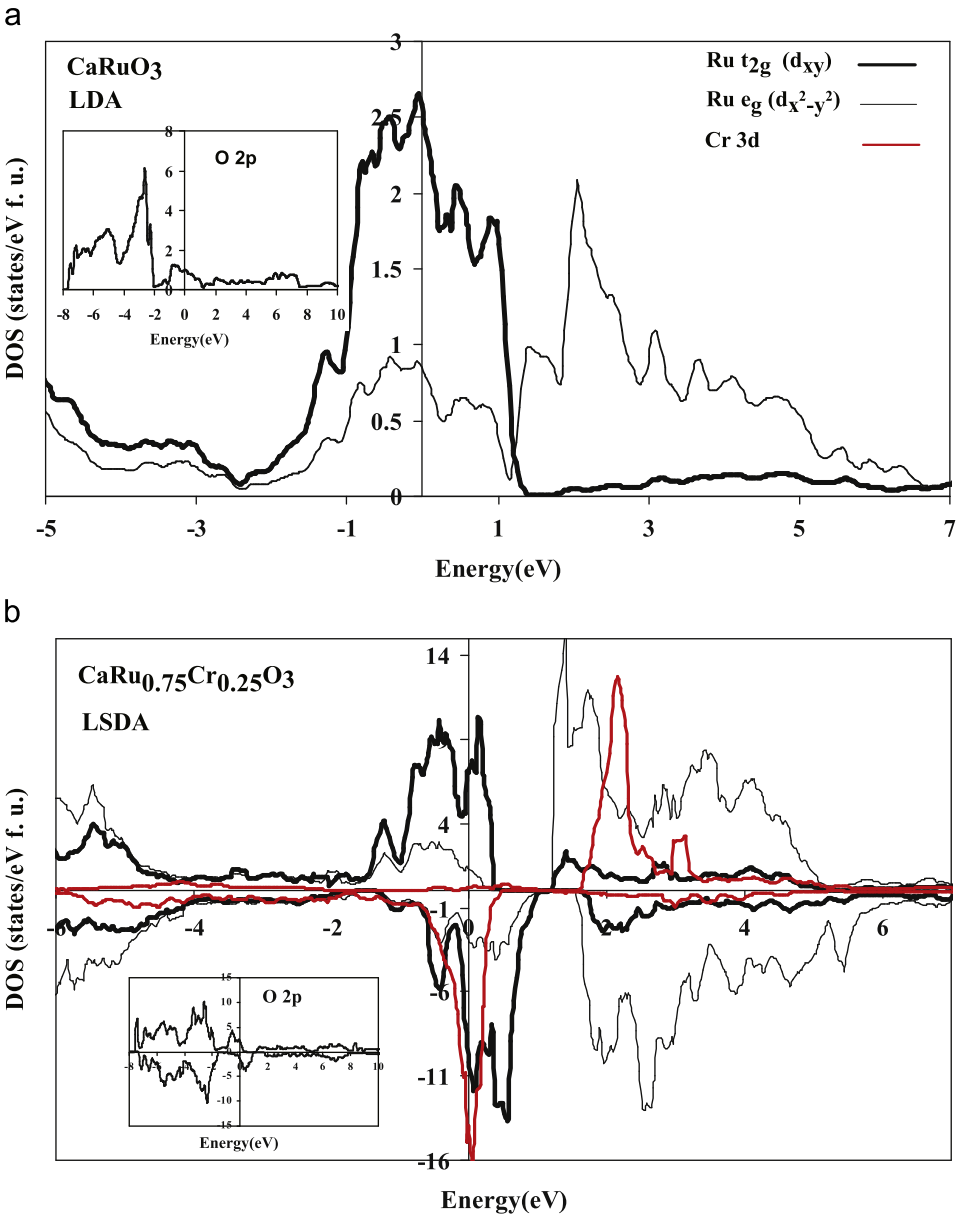


**Fig. 4.** PDOS calculated by LDA and LSDA for (a) $CaRuO_3$ and (b) $CaCr_{0.25}Ru_{0.75}O_3$. In both calculations the position of the Fermi energy is indicated at zero. The DOS results are presented for the two spins: up (down) panel corresponding to spin majority (minority). The O 2*p* PDOS are shown in the inset to Figs. 4(a) and 4(b).

($E_F$) arises primarily from the Ru 4*d* $t_{2g}$ bands. As shown in Table 2, The CEF splitting in the $Ru^{4+}$ $4d^4$ ions is so large ($E_{CEF} = E_{t_{2g\uparrow}} - E_{e_{g\uparrow}} \approx 1.5$ eV) due to the extension of the 4*d* orbitals, yielding a low spin state with $t^3_{2g\uparrow} t^1_{2g\downarrow}$. The broad and empty $e_g$ bands appear beyond 1 eV above $E_F$. The higher number of electrons in the $d_{xy}$ orbitals as compared with $d_{z^2-3r^2}$ with $t_{2g}$ and $e_g$ symmetry shows that each of the four electrons occupy the $t_{2g}$ orbitals, and the possibility of occupying the $e_g$ orbitals is very low in $Ru^{4+}$.

The results for $SrRu_{0.75}Cr_{0.25}O_3$ depicted in Fig. 3(b) are very similar to those previously reported [28]. The bands below −2 eV are predominantly of the oxygen character, while the bands crossing the Fermi level and ranging from −2 eV to about 2 eV have significant mixing between the Ru-3*d* and Cr-3*d* characters

with some small admixture of oxygen $p$ states. In order to compare the contributions from various non-equivalent Ru and Cr sites, the total Cr 3$d$ PDOS and Ru 4$d$ PDOS (only $d_{xy}$ and $d_{x^2-y^2}$) are plotted together. We have only shown the shape of the Ru(2) PDOS near the Cr ion, which depends on the Cr moment direction. The Ru $t_{2g}$ and Cr $t_{2g}$ bands are partially filled, while the Cr $e_g$ and Ru $e_g$ bands remain empty. An estimate of the $d$ occupation (orbital occupancy) is made by integrating the peak associated with the $t_{2g}$ orbitals. The occupied fraction of the peak is 0.69, corresponding to an electron count of 2.1e, intermediate between $3d^3$ $Cr^{3+}$ and $3d^2$ $Cr^{4+}$, but closer to $3d^2$ $Cr^{4+}$. Thus, the DOS results show the presence of $Cr^{4+}$ ions in these materials. The majority Ru $t_{2g}$ up spin channel is fully occupied, while the minority Ru $t_{2g}$ down spin is partially occupied, consistent with the $4d^4$ $Ru^{4+}$ configuration of Ru. There is apparently less charge transfer between Cr and the ruthenate host with creation of $Cr^{4+}$ and $Ru^{4+}$.

Substituting Ru by Cr replaces four itinerant 4$d$ electrons with two local 3$d$ electrons. Analytical results indicate that the effective exchange interaction $I$, as well as the behavior of DOS at Fermi level ($N(E_F)$), plays a crucial role in the stability of the FM state. From the extended Stoner model [54], if different kinds of atoms in a solid contribute to the DOS at Fermi level, the total Stoner $I$ for such a solid would be the average of individual $I$ with squared PDOS. So, $N(E_F)=\sum_i N_i = N(E_F)\sum_i v_i$, where, $v_i$ is the contribution of each atom in $N(E_F)$; and then total $I=\sum v_i^2 I_i$. By considering the PDOS of Ru 4$d$ and the three O 2$p$ states at Fermi level in Sr(Ca)$RuO_3$, we obtain $I=I_{Ru}v_{Ru}^2+3I_O v_O^2$. Thus, the total

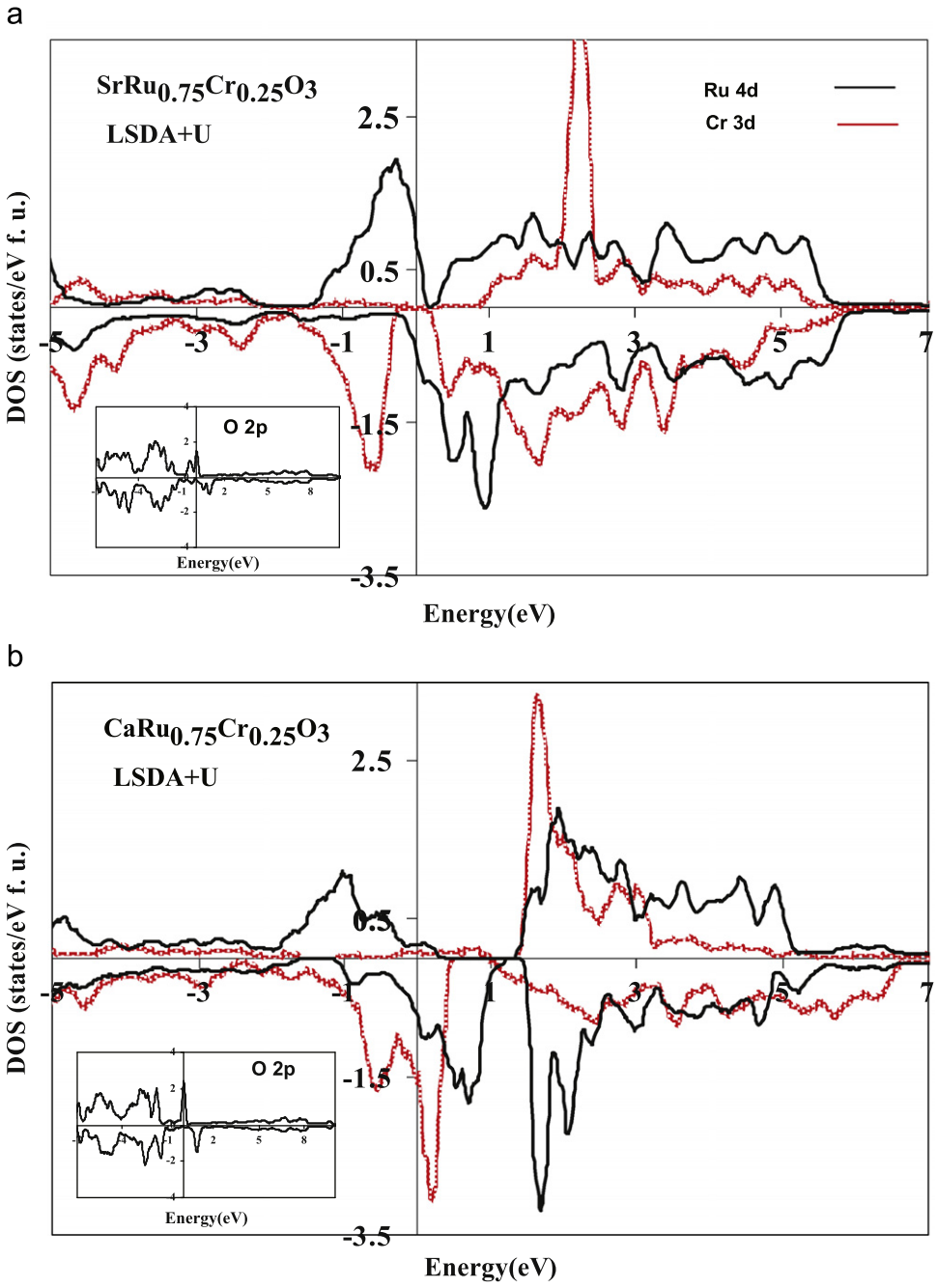


**Fig. 5.** The PDOS calculated by LSDA+$U$ for (a) $SrCr_{0.25}Ru_{0.75}O_3$ and (b) $CaCr_{0.25}Ru_{0.75}O_3$. In both calculations the position of the Fermi energy is indicated at zero. The DOS results are presented for the two spins: up (down) panel corresponding to the spin majority (minority). The O 2$p$ PDOS are shown in the inset of Figs. 5(a) and (b).

Stoner parameter for Ca(Sr)$Ru_{1-x}Cr_xO_3$ is $I = I_{Ru}v_{Ru}^2 + I_{Cr}v_{Cr}^2 + 3I_Ov_O^2$. Our DOS for $SrRu_{0.75}Cr_{0.25}O_3$ shows that the density of Ru 4*d* and Cr 3*d* states are larger than that of the O 2*p* states with $v_{Cr} > v_{Ru}$. So, the narrow $t_{2g}$ band of Cr enhances the DOS at the Fermi level, thereby providing Stoner instability in the ferromagnetism.

The ordered magnetic moment is variously reported between 0.8 and 1.6 $\mu_B$/Ru for $SrRuO_3$ and $CaRuO_3$ [3,25]. For example, the

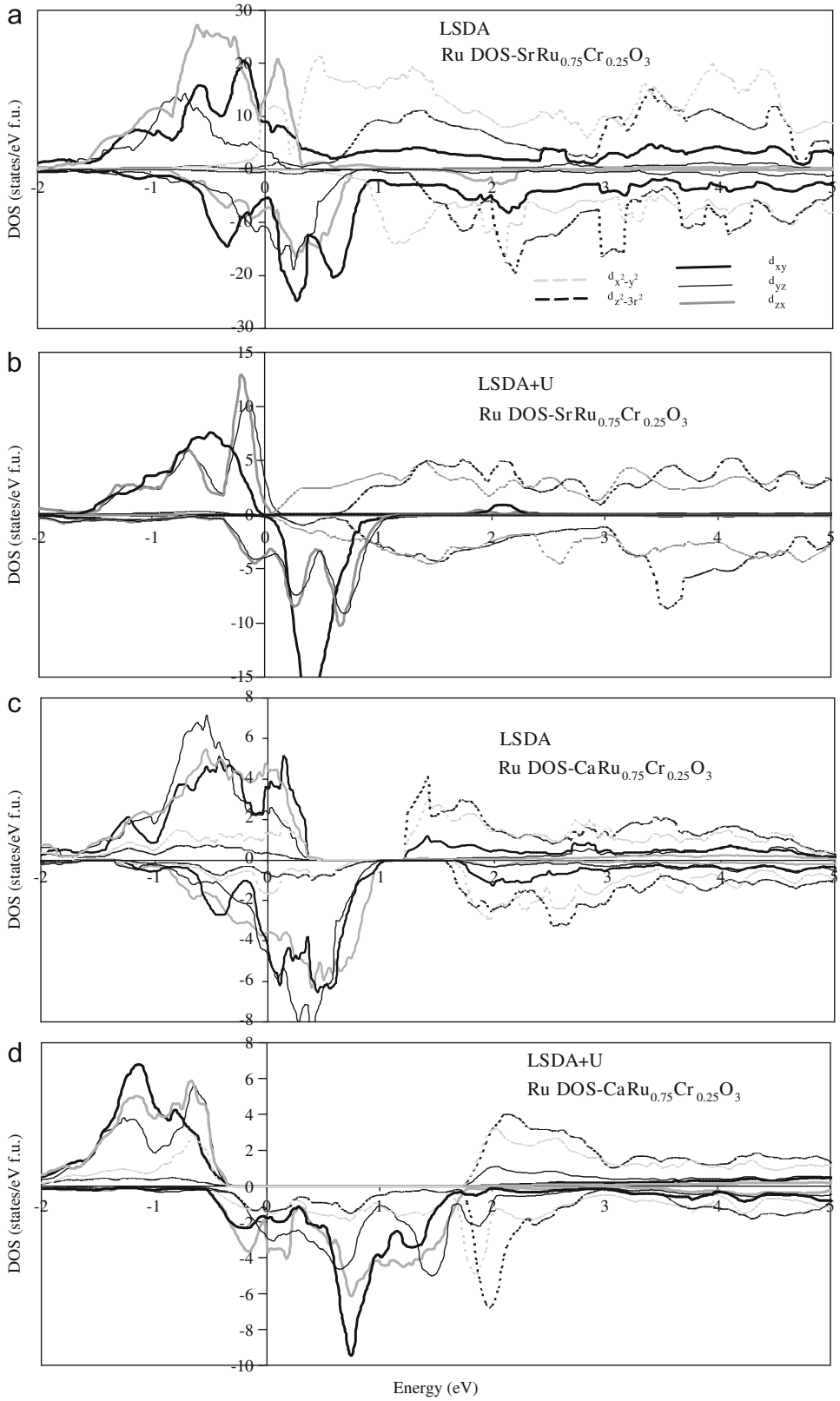


**Fig. 6.** The orbital-projected Ru DOS in Sr(Ca)$Ru_{0.75}Cr_{0.25}O_3$: (a) LSDA of $SrRu_{0.75}Cr_{0.25}O_3$, (b) LSDA+*U* of $SrRu_{0.75}Cr_{0.25}O_3$, (c) LSDA of $CaRu_{0.75}Cr_{0.25}O_3$, (d) LSDA+*U* of $CaRu_{0.75}Cr_{0.25}O_3$.

magnetic moment value of 1.4 $\mu_B$/Ru is achieved for $SrRuO_3$ in the FM ordered state. A smaller ordered magnetic moment value of 1.32 $\mu_B$/Ru is obtained for $SrRu_{1-x}Cr_xO_3$ with $x=0.05$, and this value is further reduced to 1.15 $\mu_B$/Ru with $x=0.12$ [25]. As shown in Table 3, in our LSDA calculations the Ru spin magnetic moment per atoms unit is found to be about 1.16 and 1.05 $\mu_B$/Ru for $SrRuO_3$ and $SrRu_{0.75}Cr_{0.25}O_3$, respectively, which is in the range of the experimental estimation. For $SrRu_{0.75}Cr_{0.25}O_3$, the spin

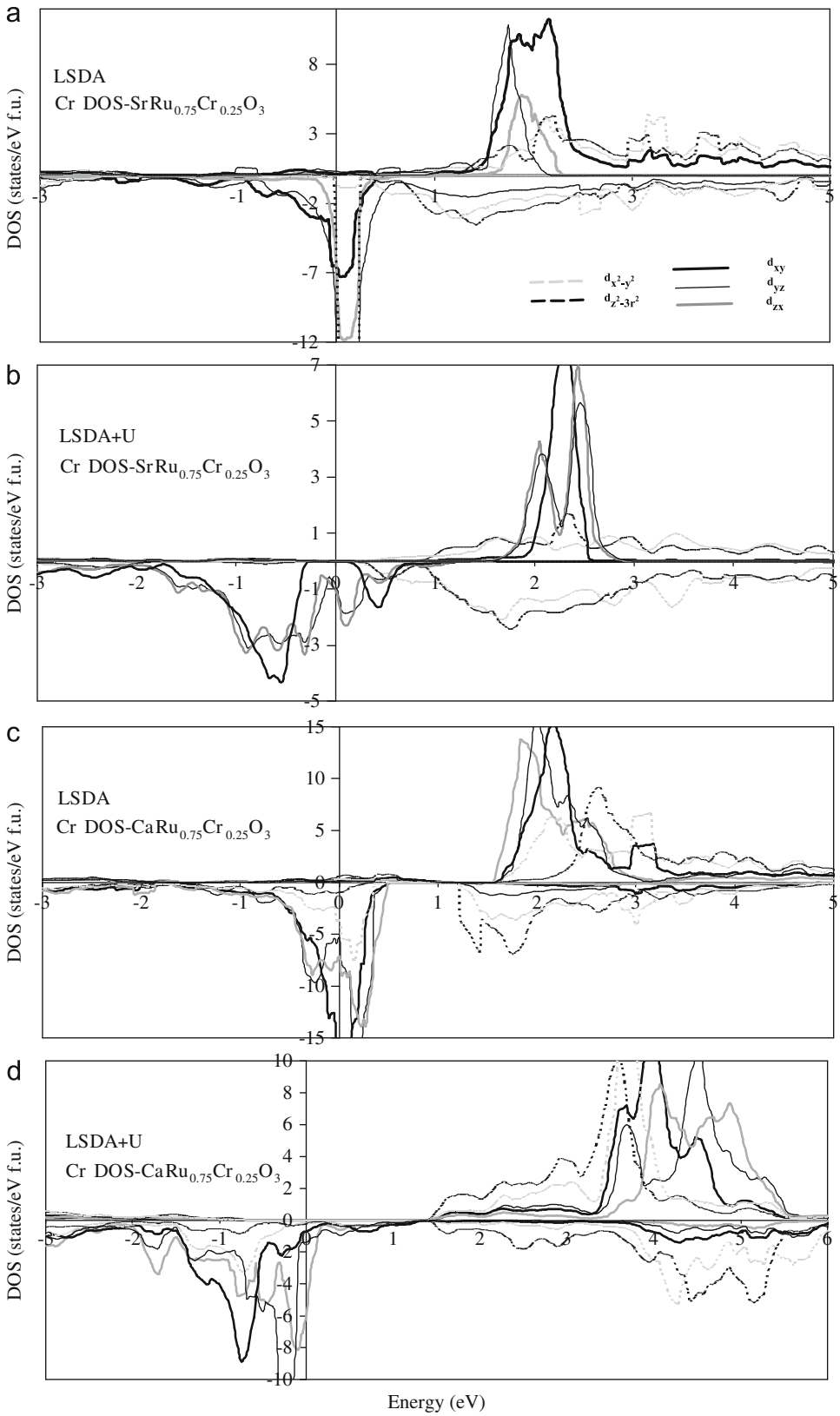


**Fig. 7.** The orbital-projected Cr DOS in Sr(Ca)$Ru_{0.75}Cr_{0.25}O_3$: (a) LSDA of $SrRu_{0.75}Cr_{0.25}O_3$, (b) LSDA+*U* of $SrRu_{0.75}Cr_{0.25}O_3$, (c) LSDA of $CaRu_{0.75}Cr_{0.25}O_3$, (d) LSDA+*U* of $CaRu_{0.75}Cr_{0.25}O_3$.

magnetic moment centered at the Cr sites is found to be 1.92 $\mu_B$, which is substantially smaller than the magnetic moment of 2–3 electrons in the $t_{2g}$ orbitals of $Cr^{3+,4+}$. This behavior of the magnetic moment results have been described in the following.

Reducing the magnetic moment of Ru in the AP calculation agrees with both the experimental magnetic moment for $SrRu_{1-x}Cr_xO_3$ and AFM alignment of Ru and Cr. For the Cr-doped $SrRuO_3$, as shown in Table 2, the Cr (Ru) site has a larger exchange splitting (ES) $\approx$2 eV ($\approx$0.8 eV) compared to the crystal field splitting $\approx$0.4 eV ($\approx$0.3 eV), while the situation is reversed for the Ru site in the $SrRuO_3$. The Ru $t_{2g}$ down spin and Ru $e_g$ up spin which are near to Fermi level, lie in the same energy range. It is then easily seen that the Ru $t_{2g\uparrow}$ state is pushed up and the Ru $t_{2g\downarrow}$ state is pushed further down by AFM coupling with the corresponding Cr states, as shown in Fig. 3(b). This behavior is very similar to the case of the $Sr_2FeMoO_6$ compound [35], where the opposite movements of Mo up and down states increase the energy separation between these two states, thereby substantially increasing the effective ES at the Mo site. So, distribution of the LSDA DOS calculation presented in Fig. 3(b) suggest that Cr-Ru hybridization is responsible for the high $T_C$ in $SrRu_{1-x}Cr_xO_3$. But, this calculation reveals a small charge transfer (presentation of $Cr^{4+}$ and $Ru^{4+}$) with small Ru ES. The presence of $Cr^{3+}$ is necessary to increase the ES and describe the mechanism providing the hybridization. Therefore, the LSDA calculation cannot completely describe the physical behavior of $SrRu_{0.75}Cr_{0.25}O_3$.

### 3.2. LDA and LSDA calculation of $CaRuO_3$ and $CaRu_{0.75}Cr_{0.25}O_3$

The DOS and PDOS calculated for the nonmagnetic $CaRuO_3$ and magnetic $CaRu_{0.75}Cr_{0.25}O_3$ solutions with the LDA and LSDA calculations are respectively shown in Figs. 4(a) and (b). The DOS intensity at $E_F$ arises primarily from the Ru $4dt_{2g}$ bands. The broad and empty $e_g$ bands appear beyond 1 eV above $E_F$. In $CaRuO_3$, there is not a strong covalency between the Ru 4*d* and O 2*p* states.

The results of the photoemission spectroscopy(PES) and *X*-ray absorption spectroscopy of $CaRuO_3$ and $SrRuO_3$ [9,10] indicate that the features close to $E_F$ has the Ru 4*d* character; the features in the range 0 to $-$2.5 eV below $E_F$ is essentially attributed to the Ru 4*d* electron excitations, and the O 2*p* contributions appear below $-$2.5 eV. Also, the maximum intensity of Ru 4*d* appears around $-$1.2 eV with negligible contributions at $E_F$ [9,10]. These features are often attributed to the localized electronic states due to electron correlations. The dominance of this apparent feature is taken as evidence for the presence of strong correlation effects [9]. In contrast, our DOS results in Fig. 4(a) by LDA calculation and also in Fig. 3(a) by LSDA calculation shows peaks at about $-$0.5 eV with considerable contributions at $E_F$ and negligible contributions beyond $-$1.0 eV. The large intensity at $E_F$ in the band structure calculations represents the extended states. This apparent disagreement in the Ru 4*d* spectral weights around the Fermi level between the LSDA band calculation and the experimental PES [9,10] indicates the importance of the electron correlation effect in the valence band which has been neglected in the LSDA calculations. Also, recent studies indicate that the correlation energy of the Ru 4*d* electrons plays an important role in the physical behaviors, especially related to the states at the Fermi level in the ternary ruthenium oxides [8,45,55].

Fig. 4(b) shows the spin up and spin down DOS of $CaRu_{0.75}Cr_{0.25}O_3$ using the optimized lattice parameters for the LSDA calculations. In contrast to the broad $e_g$ state, the sharp $t_{2g}$ state is more sensitive to substitution. The effective width of the Cr bands is significantly narrower in this system, while the Ru 4*d* electrons contributes primarily in the energies $-$2 eV to 4 eV around $E_F$. By integrating the peak associated with the $t_{2g}$ orbitals, it is evident that the Cr valence is clearly different from $3d^3$ $Cr^{3+}$; and is near $3d^2$ $Cr^{4+}$. The ES of Ru 4*d* and Cr 3*d* in the LSDA calculation is close to 0.9 and 2.2 eV, respectively. As shown in Table 3, the spin magnetic moment per atoms unit is found to be about 1.24 $\mu_B$/Ru for $CaRu_{0.75}Cr_{0.25}O_3$. Here, the spin magnetic moment centered at Cr sites is found to be 1.93 $\mu_B$. So, in $CaRu_{0.75}Cr_{0.25}O_3$, increasing the Ru magnetic moment with substitution of Cr is not consistent with the screening of electrons by hybridization. Moreover, there is low charge transfer between Cr and Ru lattice with small ES similar to the Sr-based system. In the Ca-based system, the Ru $e_g$ up spin is far from the Ru $t_{2g}$ down spin and also from the Fermi level. This is in contrast to the $SrRu_{0.75}Cr_{0.25}O_3$ case. Therefore, the electron correlation is necessary to be taken into consideration for explaining the different aspects of $Sr(Ca)Ru_{0.75}Cr_{0.25}O_3$.

### 3.3. LSDA+U calculation of $Sr(Ca)Ru_{0.75}Cr_{0.25}O_3$

As mentioned in the LSDA calculation, the small Ru ES and presence of $Cr^{4+}$, due to small charge transfer, is not consistent with the mechanism providing hybridization. Therefore, we have carried out the calculations with LSDA+*U* for $SrRu_{0.75}Cr_{0.25}O_3$, and found significant difference in the results as compared with the LSDA calculation. As shown in Fig. 5(a), the distribution of the Ru and Cr DOS calculated with LSDA+*U* is different from that in the LSDA calculation. There is apparently more charge transfer between Cr and the ruthenate host (from Cr 2*e* in $x$=0 to Cr 2.9*e* in $x$=0.25 and Ru 4*e* in $x$=0 to Ru 3.1*e* in $x$ =0.25 in the Sr based) with creation of $Cr^{3+}$ and $Ru^{5+}$, different from the LSDA case. As shown in Table 2, With the presence of Cr in the compound, the ES of the Ru $t_{2g}$ electrons increase sharply, while the energy separation between the Ru $t_{2g}$ down spin and Ru $e_g$ up spin decreases. So, the LSDA+*U* calculation confirms that in the presence of Cr in $SrRuO_3$ and hopping interactions, there is a finite coupling between the states at the Cr and Ru sites, leading to renormalization of the intra-atomic exchange strength at the Ru sites. The $Cr^{3+}$, due to its $t_{2g}^3e_g^0$ electronic configuration and close ionic size to $Ru^{4+,5+}$, favours hybridization with the $Ru^{4+,5+}$ $t_{2g}$ band, which results in a broadened bandwidth.

Fig. 5(b) shows the DOS calculated with LSDA+*U* for $CaRu_{0.75}Cr_{0.25}O_3$. For Ru, the spin up $t_{2g}$ states are fully occupied while the spin down channel is partially occupied, consistent with the $d^{3,4}$ configuration of Ru. Using the Cr 3*d* projection of the DOS for $CaRu_{0.75}Cr_{0.25}O_3$, the filling of the Cr $t_{2g}$ manifold reaches to 2.5e showing the presence of $Cr^{3+}$. The LSDA+*U* calculation shows enhancement of the magnetic moment as compared to the LSDA calculation; the magnetic moment per atom is found to be 1.36 $\mu_B$/Ru and 2.37 $\mu_B$/Cr for $CaRu_{0.75}Cr_{0.25}O_3$, which is consistent with the presence of $Cr^{3+}$. The bigger ES of Ru 4*d* and Cr 3*d* at Fermi level of $CaRu_{0.75}Cr_{0.25}O_3$ in the LSDA+*U* calculation (Fig. 5(b)) compared with that of LSDA calculation (Fig. 4(b)) shows that substitution of Cr for Ru adds the electron–electron correlation into our ruthenate system which plays an essential role in determining the electronic structure of this FM compound. When Cr is substituted, the strength of the Coulomb interaction is significantly increased due to contraction of the 3*d* wave functions when the number of localized electrons increases.

Due to the similar $Cr^{3+}$ and $Ru^{4+}$ ionic radii (0.615 Å against 0.62 Å), both Sr- and Ca-based systems retain in the orthorhombic systems. $CaRuO_3$ is a more distorted perovskite structure in comparison with $SrRuO_3$, and is close to being an insulator and very close to the magnetic–nonmagnetic transition boundary. Also, the *d*-band width is narrower for $CaRuO_3$ than for $SrRuO_3$ [29]. This properties suggest that the electron–electron

correlation plays an essential role in determining the correct electronic structure of $CaRu_{0.75}Cr_{0.25}O_3$. The low ES and high Ru magnetic moment resulted from the LSDA calculation of $CaRu_{0.75}Cr_{0.25}O_3$ show that the mechanism is different in the Ca-based systems as compared with the Sr-based systems. The LSDA+$U$ calculation results in high ES, presence of $Cr^{3+}$, and higher magnetic moment in $CaRu_{0.75}Cr_{0.25}O_3$. For low concentration and near half filling ($Cr^{4+,3+}$ and $Ru^{4+,5+}$), the strong hybridization between the spin-polarized Cr $t_{2g}$ orbitals and O 2$p$ orbitals associated with the Ru 4d$t_{2g}$–O 2$p$ band are much reduced by $U$, and this repulsion between electrons tend to keep the localized spins from overlapping. In spite of the presence of $Cr^{3+}$ and AFM alignment with the Ru ions in the compound, due to high on-site Coulomb repulsion, screening of Ru $t_{2g}$ electrons decrease, which is consistent with both high Ru ES and high Ru magnetic moment. So, low screening strengthens the exchange coupling between the local spins, and hence increases $T_C$. Also, there is apparently more charge transfer between Cr and the ruthenate host as compared with the LSDA calculation. This charge transfer eliminates one electron in the Ru 4$d$ shell, which would interrupt the itinerancy of the Ru electrons.

In order to obtain more insight into the Ru 4$d$ and Cr 3$d$ states in $Sr(Ca)Ru_{0.75}Cr_{0.25}O_3$, we show the orbital-projected DOS in Fig. 6 for Ru and in Fig. 7 for Cr both with and without correlation. As shown in Fig. 6, for both the Sr- and Ca-based systems, the Ru $t_{2g}$ orbitals lie close to $E_F$ while the Ru $e_g$ orbitals spreads out over a wide energy range. Another notable aspect of the DOS profiles in $Sr(Ca)Ru_{0.75}Cr_{0.25}O_3$ is that each of the Ru $t_{2g}$ and Ru $e_g$ orbitals in the LSDA calculation for both Sr- and Ca-based systems (Figs. 6(a) and 6(c)) has different DOS profile depending upon their orientation, whereas the distribution of the DOS curves for LSDA+$U$ calculation (Figs. 6(b) and 6(d)) does not differ much.

The valance bands of Cr in the LSDA calculation for both Ca- and Sr-based compounds are of predominantly $d_{xz}$, $d_{xy}$, and $d_{zy}$ characters with the same occupancies (Figs. 7(a) and 7(c)), whereas those of the LSDA+$U$ calculation of $Sr(Ca)Ru_{0.75}Cr_{0.25}O_3$ (Figs. 7(b) and 7(d)) are of the mainly $d_{yz}$ and $d_{zx}$ features with the third $d_{xy}$ orbital full. The inclusion of correlation shows that each Cr has approximately 2–3 spin-down electron occupying one $d_{xy}$ and mixed $d_{yz}$ and $d_{zx}$ orbitals. Such an orbital ordering state results from the fluctuations of occupancies among the three fold Cr $t_{2g}$ orbitals provided in LSDA+$U$. Importantly, the formation of the Cr 3$d$ orbital ordering state occurs only when the on-site Coulomb interaction $U$ and the structural distortion are taken into account simultaneously. Calculations in the absence of either the on-site $U$ or lattice distortion gives rise to a normal ground state with the spin down electron distributed evenly onto the three $t_{2g}$ orbitals. So, our results indicate that the electron correlation plays an important role in the magnetic and electrical behaviors of both Sr- and Ca-based systems. Inclusion of correlation in the Sr-based confirms that hybridization is responsible for the high $T_C$ in this system. Influence of the Coulomb repulsion in the Ca-based system is more than in the Sr-based system due to its more distorted structure. Because of the high electron correlation, the mechanism is different in the Ca-based system, and low screening strengthens the exchange coupling between the local spins, leading to high $T_C$.

## 4. Summary

Our computations reveal that the electron correlation plays an important role in the physical behaviors of both Sr- and Ca-based systems. The electronic structure calculations show that different mechanisms are responsible for the increase of $T_C$ in the two isostructural $Sr(Ca)Ru_{1-x}Cr_xO_3$ systems. The large increase of $T_C$ in $SrRu_{1-x}Cr_xO_3$ is due to AFM coupling between the Cr and Ru states, which induces large ES; applying electron correlation improves the mechanism providing hybridization in the Sr-based systems. The decrease in the Ru–O(1)–Ru and Ru–O(2)–Ru bond angle with increasing $x$ suggests that distortion and rotation of $RuO_6$ octahedra retain in the Ca-based systems. In $CaRu_{1-x}Cr_xO_3$, due to the more structural distortion, the inclusion of correlations causes a significant role in evaluating the magnetic properties of $CaRu_{1-x}Cr_xO_3$. The LSDA+$U$ calculations, which is consistent with the high Ru and Cr magnetic moments, suggest more charge transfer from Ru to Cr as compared to the LSDA calculation. The creation of $Cr^{3+}$ and $Ru^{5+}$ due to more charge transfer describes the insulating behavior of the high Cr-doped systems. So, in $CaRu_{1-x}Cr_xO_3$, due to low screening of the Ru $t_{2g}$ electrons, the inclusion of correlations strengthens the exchange coupling between the local spins, leading to high $T_C$.

## Acknowledgments

We would like to acknowledge fruitful discussions with R. Mozaffari, R. Noorafkan and S. Fallahi. This work was supported in part by the National Centre of Excellence in Complex Systems and Condensed Matter (CSCM) of the Department of Physics at Sharif University of Technology (http://www.cscm.ir).

## References

[1] Y. Maeno, H. Hashimoto, K. Yoshida, S. Nishizaki, T. Fujita, J.G. Bednorz, F. Lichtenberg, Nature (London) 372 (1994) 532.
[2] P. Khalifah, I. Ohkubo, H. Christen, D. Mandrus, Phys. Rev. B 70 (2004) 134426;
Y.S. Lee, J. Yu, J.S. Lee, T.W. Noh, T.H. Gimm, H.Y. Choi, C.B. Eom, Phys. Rev. B 66 (2002) 041104(R).
[3] G. Cao, S. McCall, M. Shepard, J.E. Crow, R.P. Guertin, Phys. Rev. B 56 (1997) 321.
[4] K. Maiti, R.S. Singh, Phys. Rev. B 71 (2005) 161102(R);
K. Maiti, Phys. Rev. B 73 (2006) 235110.
[5] D.J. Singh, J. Appl. Phys. 79 (1996) 4818.
[6] I.I. Mazin, D.J. Singh, Phys. Rev. B 56 (1997) 2556.
[7] J.S. Ahn, J. Bak, H.S. Choi, T.W. Noh, J.E. Han, Y. Bang, J.H. Cho, Q.X. Jia, Phys. Rev. Lett. 82 (1999) 5321.
[8] A.V. Puchkov, M.C. Schabel, D.N. Basov, T. Startseva, G. Cao, T. Timusk, Z.-X. Shen, Phys. Rev. Lett. 81 (1998) 2747.
[9] J. Okamoto, T. Mizokawa, A. Fujimori, I. Hase, M. Nohara, H. Takagi, Y. Takeda, M. Takano, Phys. Rev. B 60 (1999) 2281.
[10] J. Park, S.J. Oh, J.-H. Park, D.M. Kim, C.-B. Eom, Phys. Rev. B 69 (2004) 085108.
[11] L. Klein, L. Antognazza, T.H. Geballe, M.R. Beasley, A. Kapitulnik, Phys. Rev. B 60 (1999) 1448.
[12] P. Kostic, Y. Okada, N.C. Collins, Z. Schlesinger, J.W. Reiner, L. Klein, A. Kapitulnik, T.H. Geballe, M.R. Beasley, Phys. Rev. Lett. 81 (1998) 2498.
[13] J.S. Dodge, C.P. Weber, J. Corson, J. Orenstein, Z. Schlesinger, J.W. Reiner, M.R. Beasley, Phys. Rev. Lett. 85 (2000) 4932.
[14] R. Vidya, P. Ravindran, A. Kjekshus, H. Fjellvag, B.C. Hauback, J. Solid State Chem. 177 (2004) 146.
[15] J.M. Rondinelli, N.M. Caffrey, S. Sanvito, N.A. Spaldin, Phys. Rev. B 78 (2008) 155107.
[16] G. Cao, S. McCall, J. Bolivar, M. Shepard, F. Freibert, P. Henning, J.E. Crow, T. Yuen, Phys. Rev. B 54 (1996) 15144.
[17] G. Cao, F. Freibert, J.E. Crow, J. Appl. Phys. 81 (1997) 3884.
[18] G. Cao, S. Chikara, X.N. Lin, E. Elhami, V. Durairaj, P. Schlottmann, Phys. Rev. B 71 (2005) 035104.
[19] T. He, R.J. Cava, J. Phys. Condens. Matter 13 (2001) 8347.
[20] L. Pi, A. Maignan, R. Retoux, B. Raveau, J. Phys. Condens. Matter 14 (2002) 7391.
[21] K.W. Kim, J.S. Lee, T.W. Noh, S.R. Lee, K. Char, Phys. Rev. B 71 (2005) 125104.
[22] D.A. Crandles, M.M. Yazdanian, F.S. Razavi, J. Phys. D Appl. Phys. 39 (2006) 6.
[23] A. Mamchik, I. Wei Chen, Phys. Rev. B 70 (2004) 104409.
[24] A. Gupta, B.W. Hussey, T.M. Shaw, Mater. Res. Bull. 31 (1996) 1463.
[25] Z.H. Han, J.I. Budnick, W.A. Hines, B. Dabrowski, S. Kolesnik, T. Maxwell, J. Phys. Condens. Matter 17 (2005) 1193.
[26] B. Dabrowski, S. Kolesnik, O. Chmaissem, T. Maxwell, M. Avdeev, P.W. Barnes, J.D. Jorgensen, Phys. Rev. B 72 (2005) 054428.
[27] V. Durairaj, S. Chikara, X.N. Lin, A. Douglass, G. Cao, P. Schlottmann, E.S. Choi, R.P. Guertin, Phys. Rev. B 73 (2006) 214414.
[28] D. Kasinathan, D.J. Singh, Phys. Rev. B 74 (2006) 195106.
[29] J.B. Goodenough, J.M. Longo, J.A. Kafalas, Mater. Res. Bull. 3 (1968) 471.
[30] J.B. Goodenough, Czech. J. Phys. B 17 (1967) 304.

[31] S.V. Streltsov, M.A. Korotin, V.I. Anisimov, D.I. Khomskii, Phys. Rev. B 78 (2008) 054425.
[32] Y. Kurtulus, R. Dronskowski, G.D. Samolyuk, V.P. Antropov, Phys. Rev. B 71 (2005) 014425.
[33] J. Rusz, I. Turek, M. Divis, Phys. Rev. B 71 (2005) 174408.
[34] A. Sharma, W. Nolting, Phys. Rev. B 78 (2008) 054402.
[35] D.D. Sarma, P. Mahadevan, T. Saha-Dasgupta, S. Ray, A. Kumar, Phys. Rev. Lett. 85 (2000) 2549.
[36] L.M. Sandratskii, P. Bruno, J. Kudrnovsky, Phys. Rev. B 69 (2004) 195203.
[38] E. Stoner, Proc. R. Soc. London Ser. A 154 (1936) 656.
[39] V.I. Anisimov, J. Zaanen, O.K. Andersen, Phys. Rev. B 44 (1991) 943.
[40] E. Sjostedt, L. Nordstrom, D.J. Singh, Solid State Commun. 114 (2000) 15; G.K.H. Madsen, P. Blaha, K. Schwarz, E. Sjostedt, L. Nordstrom, Phys. Rev. B 64 (2001) 195134.
[41] K. Schwarz, P. Blaha, Comput. Mater. Sci. 28 (2003) 259.
[42] D. Singh, Phys. Rev. B 43 (1991) 6388.
[43] M.V. Rama Rao, V.G. Sathe, D. Sornadurai, B. Panigrahi, T. Shripathi, J. Phys. Chem. Solids 62 (2001) 797–806.
[44] A.I. Liechtenstein, V.I. Anisimov, J. Zaanen, Phys. Rev. B 52 (1995) R5467; V.I. Anisimov, F. Aryasetiawan, A.I. Lichtenstein, J. Phys. Condens. Matter 9 (1997) 767.
[45] J.C. Slater, Quantum Theory of Molecules and Solids, vol. IV, McGraw-Hill, New York, 1974.
[46] M.R. Norman, A.J. Freeman, Phys. Rev. B 33 (1986) 8896; A.K. McMahan, R.M. Martin, S. Satpathy, Phys. Rev. B 38 (1988) 6650.
[47] I.V. Solovyev, P.H. Dederichs, Phys. Rev. B 49 (1994) 6736.
[48] V.I. Anisimov, O. Gunnarsson, Phys. Rev. B 43 (1991) 7570.
[49] G.K.H. Madsen, P. Novak, Europhys. Lett. 69 (2005) 777.
[50] B.J. Kennedy, B.A. Hunter, Phys. Rev. B 58 (1998) 653.
[51] A. Callaghan, C.W. Moeller, R. Ward, Inorg. Chem. 5 (1966) 1572.
[52] H. Kobayashi, M. Nagata, R. Kanno, Y. Kawamoto, Mater. Res. Bull. 29 (1994) 1271.
[53] H. Nakatsugawa, E. Iguchi, Y. Oohara, J. Phys. Condens. Matter 14 (2002) 415.
[54] P.M. Marcus, V.L. Moruzzi, Phys. Rev. B 38 (1988) 6949.
[55] J.S. Lee, Y.S. Lee, T.W. Noh, K. Char, J. Park, S.-J. Oh, J.-H. Park, C.B. Eom, T. Takeda, R. Kanno, Phys. Rev. B 64 (2001) 245107.